Mechanism and Machine Theory 146 (2020) 103722

Contents lists available at ScienceDirect

Mechanism and Machine Theory

journal homepage: www.elsevier.com/locate/mechmachtheory

Research paper

The influence of coordinates in robotic manipulability analysis☆

Johannes Lachner[a,b,*], Vincenzo Schettino[b], Felix Allmendinger[b], Mario Daniele Fiore[b], Fanny Ficuciello[c], Bruno Siciliano[c], Stefano Stramigioli[a]

[a] Faculty of Electrical Engineering, Mathematics and Computer Science, University of Twente, Enschede, The Netherlands
[b] KUKA Deutschland GmbH, Zugspitzstrasse 140, Augsburg, Germany
[c] PRISMA Lab, Department of Electrical Engineering and Information Technology, University of Naples Federico II, via Claudio 21, Naples, 80125, Italy

ARTICLE INFO

Article history:
Received 30 March 2019
Revised 25 October 2019
Accepted 19 November 2019

Keywords:
Manipulability ellipsoids
Coordinate invariance
Tensor analysis
Metrics

ABSTRACT

Coordinates play an essential role in the description of real world objects and physical processes. In robotics, coordinates are used to describe the kinematic structure and the kinematic and dynamic behavior. The description mostly takes place in charts, assigned by the observer of the robotic system. However, it is crucial that the described physical process does not depend on the coordinate choice of the observer. In this work we show the relation between coordinates and manipulability analysis. Manipulability measures are dependent of joint coordinates of the robot and task coordinates in the workspace of the robot. Both relations can be analyzed with tensor geometry. We remove the dependency on joint coordinates through the use of an appropriate metric. With the help of tensor contraction, the resulting induced metric in the workspace can be transformed into a coordinate invariant matrix. After applying eigenvalue decomposition on this matrix, we can visualize the dynamic manipulability of a robot as a coordinate invariant ellipsoid.

1. Introduction

Manipulability is not a well-defined mathematical concept. Nevertheless, it is important to have a measure on how well a robot can perform a given task. A lot of authors have proposed many different manipulability measures. There are different objectives behind the measures: some focus on control [1–4], some on kinematic analysis [5–8].

Manipulability measures are related to two kind of coordinates: joint coordinates and task coordinates. Joint coordinates describe the kinematic structure, whereas task coordinates are used to program the movement of the robot in the workspace.

Manipulability measures must be independent of the choice of joint coordinates. For example, a mobile manipulator is often modeled with different joint types. Mostly, rotational parameters are assigned for the robot arm and the base is described with translational parameters. A lot of manipulability measures can only be applied when every joint coordinate has the same unit. Therefore, no statement about the manipulability of the entire mobile robot can be found. A common

☆ This project has received funding from the European Unions Horizon 2020 research and innovation programme under Grant Agreement No. 688188
* Corresponding author.
E-mail address: j.lachner@utwente.nl (J. Lachner).

https://doi.org/10.1016/j.mechmachtheory.2019.103722
0094-114X/

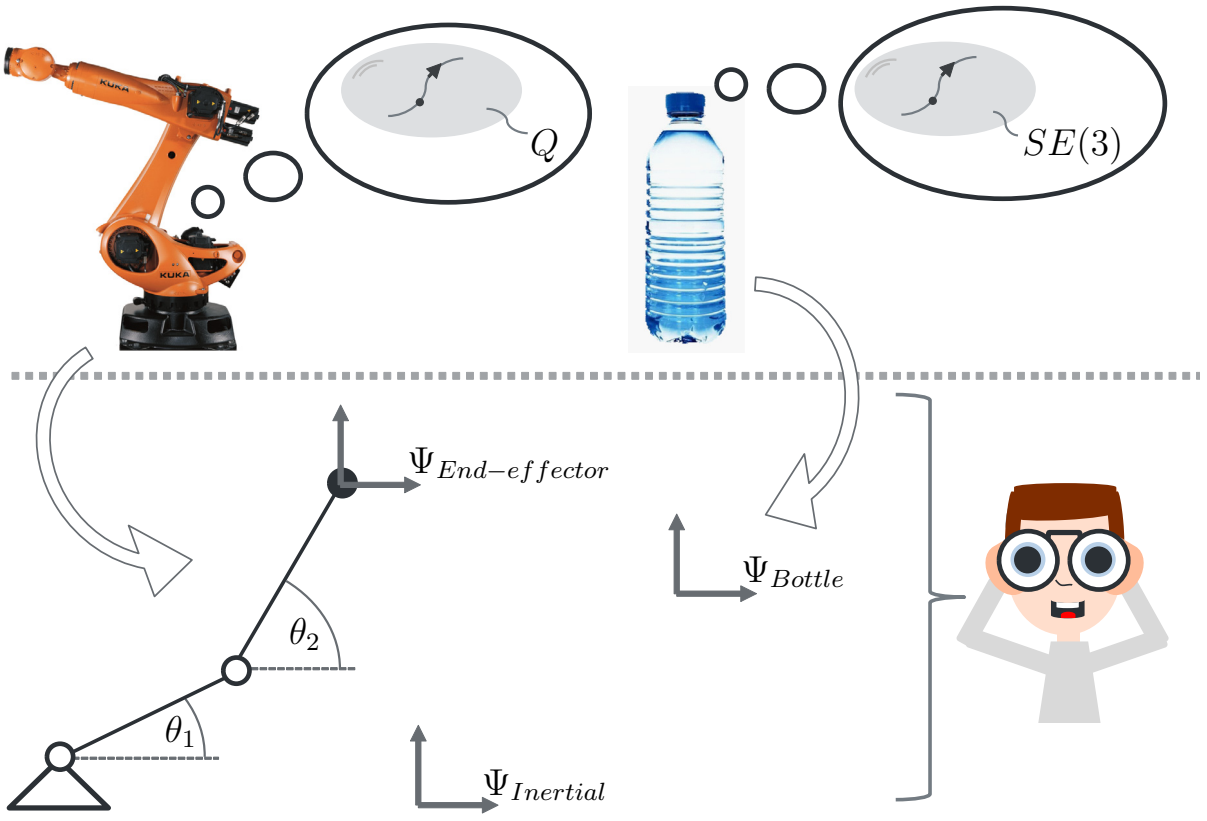

Fig. 1. Separation between real world objects and observer-centric view. In the upper part, the two physical objects "robot" and "bottle" are illustrated. They are represented as elements on differentiable manifolds. In the lower part of the picture, the objects are charted by an observer.

approach is to modify the matrix elements to characteristic lengths [9,10]. The dependency on joint coordinates can be removed, by changing entries with different units to dimensionally homogeneous components. Hereby, the physical meaning gets lost.

Robotic applications are programmed by aligning two task coordinates, e.g. one body fixed coordinate on the robot end-effector and a stationary coordinate in the workspace. The manipulability of the robot can then be described as a function of the body-fixed task coordinate and the robot posture. An example is screw fastening, where the manipulability along the screw axis is of interest. In this example, the use of task coordinates might be applicable. However, this is not always the case. Imagine a robot grasping a bottle and pouring water in a glass. What would be an appropriate task coordinate to represent the manipulability?

The main aim of this paper is to show the relations between manipulability analysis and both types of coordinates. The derivation will start with an analysis of the matrix $\boldsymbol{J(q)J(q)^T}$. We will show that different *Velocity Manipulability Ellipsoids* arise for one and the same robot. The reasons can be illustrated with the help of tensor contraction. In a further step, tensors are used to derive a coordinate invariant manipulability measure. The novelty of this paper is to define manipulability as a property of the physical object and not as a property of the task coordinate on the object (cf. Fig. 1). We will show that for rotational tasks, we can remove the dependency on both kind of coordinates.

2. Manipulability ellipsoids

Consider a robot with n-number of joint coordinates and m-number of task coordinates.

Manipulability measures are strongly related to the Jacobian matrix $\boldsymbol{J(q)}$. $\boldsymbol{J(q)} \in \mathbb{R}^{m\times n}$ maps the joint velocities $\dot{\boldsymbol{q}} \in \mathbb{R}^n$ to velocities in Cartesian space:

$$\dot{\boldsymbol{x}} = \boldsymbol{J}(\boldsymbol{q})\dot{\boldsymbol{q}}, \tag{1}$$

with $\dot{\boldsymbol{x}} \in \mathbb{R}^m$ being the task velocity. The columns of $\boldsymbol{J(q)}$ are the joint twists with respect to the task coordinate Ψ_{Task} [11]. For manipulability analysis, $\boldsymbol{J(q)}$ itself was examined in [12,13]. This shows how manipulability analysis is linked to the choice of Ψ_{Task}.

2.1. Velocity Manipulablity Ellipsoid

Another commonly examined matrix is the matrix $\boldsymbol{J(q)J(q)^T}$, e.g. in the work of [14–17] and more recently used in [18–21]. It is the core of the *Velocity Manipulability Ellipsoid*, [22,23] and is often recommended for manipulability analysis of kinematically redundant robots ($n > m$).

2.1.1. Derivation of $\mathbf{J(q)J(q)^T}$

The derivation of this ellipsoid starts by visualizing the velocities $\dot{\boldsymbol{q}}$ as a sphere. The used sphere equation is

$$\dot{\boldsymbol{q}}^T\dot{\boldsymbol{q}} = 1. \tag{2}$$

In the kinematically redundant case, there are infinitely many solutions of $\dot{\boldsymbol{q}}$ to produce a desired Cartesian velocity. To find a solution, one has to minimize a cost function. A typical choice is

$$g(\dot{\boldsymbol{q}}) = \frac{1}{2}\dot{\boldsymbol{q}}^T\boldsymbol{W}\dot{\boldsymbol{q}}, \tag{3}$$

with $\boldsymbol{W} \in \mathbb{R}^{n\times n}$ being a symmetric positive definite weighting matrix. The solution obtained is a *Generalized Inverse* of $\boldsymbol{J(q)}$:

$$\boldsymbol{J(q)^{\#} = W^{-1}J(q)^T\left(J(q)W^{-1}J(q)^T\right)^{-1}}. \tag{4}$$

Choosing $\boldsymbol{W}$ equal to the Identity matrix yields the *Moore – Penrose Inverse* $\boldsymbol{J(q)^{\dagger}}$ [24]. Eq. (1) can therefore be "inverted" to:

$$\dot{\boldsymbol{q}} = \boldsymbol{J(q)^{\dagger}}\dot{\boldsymbol{x}}. \tag{5}$$

Substituting Eq. (5) in Eq. (2) results in an ellipsoid in the Cartesian Space:

$$\dot{\boldsymbol{x}}^T\left(\boldsymbol{J(q)J(q)^T}\right)^{-1}\dot{\boldsymbol{x}} = 1. \tag{6}$$

The shape and orientation of the ellipsoid is determined by the matrix $\boldsymbol{J(q)J(q)^T}$.

2.1.2. Specific aspects of $\boldsymbol{J(q)J(q)^T}$

The matrix $\boldsymbol{J(q)J(q)^T}$ is not independent of joint coordinates. In Fig. 2, a robot with different sets of joint coordinates is illustrated. Assigning different sets for the same robot yields different values in $\boldsymbol{J(q)J(q)^T}$ and in its eigenvalue decomposition. If the set of coordinates is chosen such that not all coordinates bear the same unit, the matrix product $\boldsymbol{J(q)J(q)^T}$ even cannot be calculated, because a mismatch of units arises (cf. previous work of [25,26] and Appendix C). This has the consequence that $\boldsymbol{J(q)J(q)^T}$ cannot be computed for a mobile robot, without separating base and robot arm. Moreover, the derivation of Eq. (6) needs an inversion of $\boldsymbol{J(q)}$. As it can be seen in Eq. (4), any positive definite weighting matrix can be chosen for non-square matrices $\boldsymbol{J(q)}$. Without a meaningful choice, the resulting inverse of $\boldsymbol{J(q)}$ incorporates no physical meaning [27]. This must be considered when applying $\boldsymbol{J(q)J(q)^T}$ for the manipulability analysis of a kinematically redundant robot, for which it is often recommended.

The shape and orientation of the Velocity Manipulability Ellipsoid is determined by the lengths and directions of the semi-axes [22]. The axes point along the direction of the eigenvectors of $\boldsymbol{J(q)J(q)^T}$. The length of the axes is determined by the square roots of the eigenvalues of $\boldsymbol{J(q)J(q)^T}$.

Fig. 3 shows different manipulability ellipsoids for one and the same robot. One ellipsoid has a randomly chosen weighting matrix $\boldsymbol{W_{rand}}$, with values given in Appendix C. This illustrates how the obtained results critically depend on the choice of joint coordinates and the weighting matrix $\boldsymbol{W}$: one observer choice might infer high manipulability and another poor manipulability.

2.2. Tensors for manipulability analysis

Tensors represent real world objects. They are entities defined on differentiable manifolds [28,29]. The joint configuration of the robot is a point on the manifold Q. The homogeneous transformation of one point on the manipulator is a point on the manifold $SE(3)$. To describe a physical state of the robot, usually charts are taken for each manifold. Charted elements of Q form the joint space $\mathbb{Q} \cong \mathbb{R}^n$ and charted elements of $SE(3)$ form the workspace $\mathbb{W} \cong \mathbb{R}^m$. The resulting coordinates selected by the observer are then used for description (cf. Fig. 1).

Joint coordinates are represented in $\mathbb{R}^n$ and task coordinates are represented in $\mathbb{R}^m$. To describe the magnitude of the velocity in Ψ_{Task}, mostly an inner product with Euclidean metric is used. Therefore, one is restricted to the use of orthonormal frames. In the remainder of the paper, we will see that tensors don't have such restrictions.

2.2.1. Tensor analysis

In the observer-centric description, no separation between vectors and co-vector is made. Therefore, important information about the underlying elements gets lost. Tensor analysis separates these elements according to their transformation properties (cf. Appendix A). Using the rules of tensor contraction, the correctness of mathematical equations can be checked (cf. Appendix B). Literature on tensors can be found in [28–30].

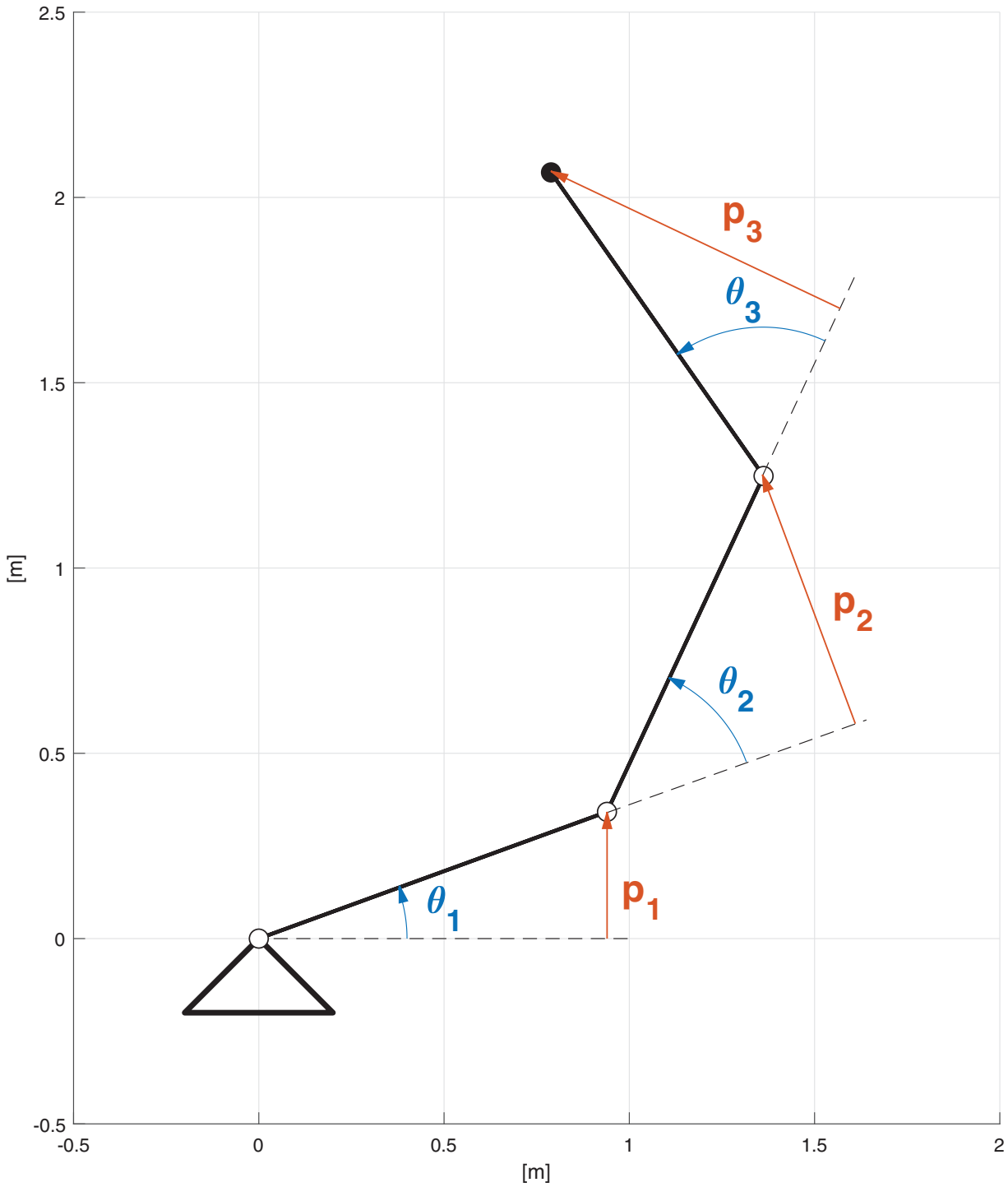

Fig. 2. 3-DOF planar robot with different set of joint coordinates: Blue set (θ_1, θ_2, θ_3) with unit [*rad*] and red set (p_1, p_2, p_3) with unit [*m*]. The values of the joint coordinate sets can be seen in Appendix C. (For interpretation of the references to colour in this figure legend, the reader is referred to the web version of this article.)

2.2.2. Eigenvalues of tensors and choice for metric

In tensor language, the eigenvalue problem is

$$\boldsymbol{T}^{\boldsymbol{a}}_{\boldsymbol{m}}\boldsymbol{u}^{\boldsymbol{m}} = \boldsymbol{\lambda}\boldsymbol{u}^{\boldsymbol{a}}. \tag{7}$$

It can be seen that this equality only holds for tensors of type $\boldsymbol{T}^{\boldsymbol{a}}_{\boldsymbol{m}}$.

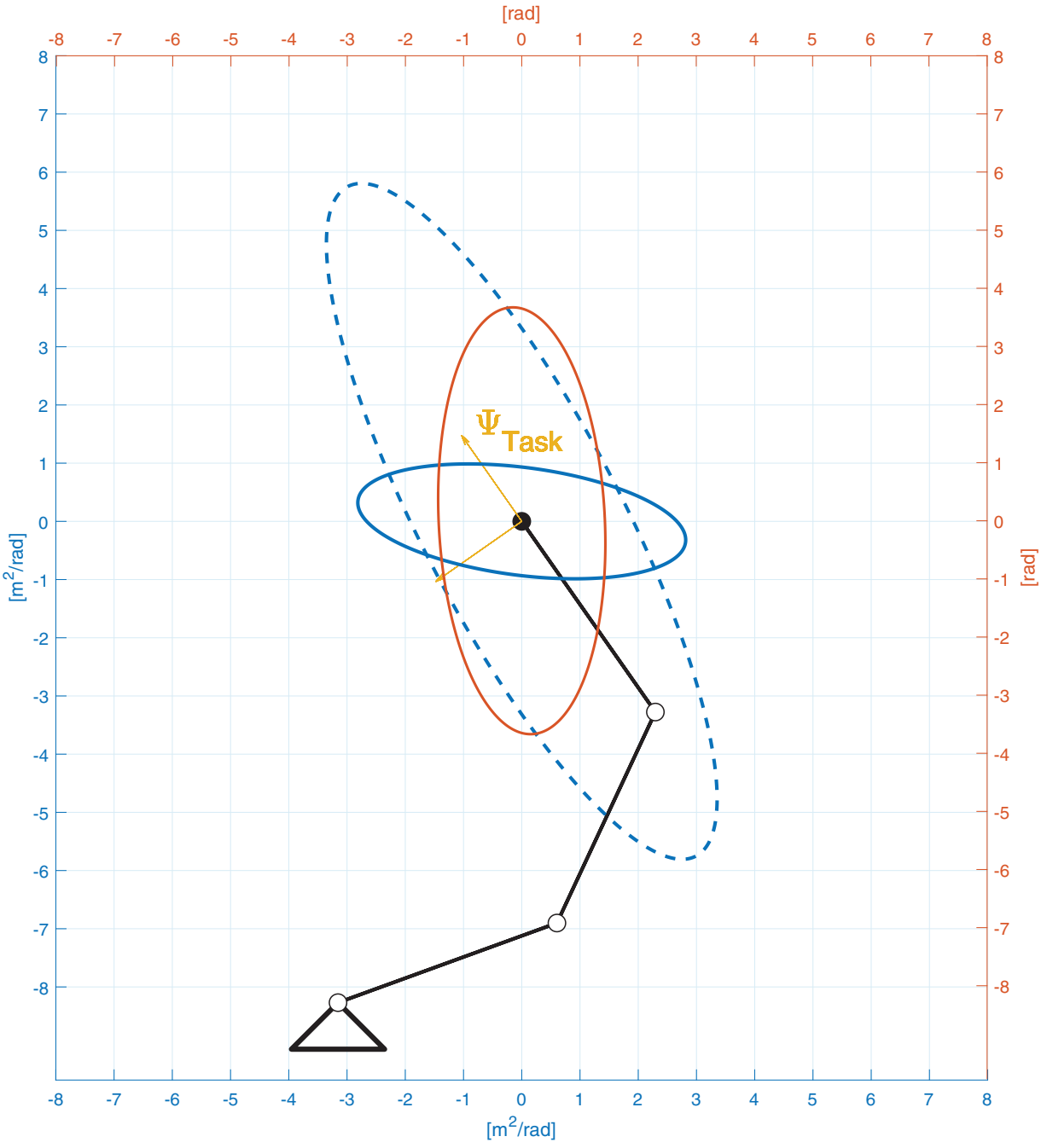

Fig. 3. Velocity manipulability ellipsoids: blue ellipsoids for joint coordinate set (θ_1, θ_2, θ_3) and red ellipsoid for joint coordinate set (p_1, p_2, p_3). The ellipsoids drawn solid have $\boldsymbol{W = I}$. The blue ellipsoid with dotted line has $\boldsymbol{W = W_{rand}}$. $\boldsymbol{W_{rand}}$ and the values for the axes lengths and axes directions can be seen in Appendix C. (For interpretation of the references to colour in this figure legend, the reader is referred to the web version of this article.)

$\boldsymbol{J(q)J(q)^T}$ is a matrix of type $\boldsymbol{T_{am}}$ and Eq. (7) has to be rewritten:

$$\boldsymbol{T_{am}u^m = \lambda u^a}, \tag{8}$$

We can rewrite Eq. (6) to

$$\boldsymbol{\dot{x}^T (J(q)IJ(q)^T)^{-1} \dot{x}} = 1. \tag{9}$$

For the core of the quadratic form in Eq. (9), $\boldsymbol{I}$ is the used metric and is therefore restricted to the use of Euclidean coordinates in the observer world. Only for Euclidean norm, Eq. (8) is correct and therefore $\boldsymbol{T_{am} = T_m^a}$.

Since joint coordinates are not related to Euclidean metric, we will have to derive an appropriate metric for Eq. (9) and transform it to a tensor of type $\boldsymbol{T_m^a}$.

3. Coordinate invariant manipulability analysis

Manipulability represents a physical characteristic of a robot: the robot can produce certain accelerations and forces in respective workspace directions. Uncharted accelerations and forces are elements on a manifold. To speak about the length of an element, a metric has to be defined. We will use appropriate metrics for the $\mathbb{Q}$-space and $\mathbb{W}$-space, to remove the dependency on joint coordinates and task coordinates.

3.1. Invariance on joint coordinates

The two vectors $\dot{\boldsymbol{q}}$ and $\dot{\boldsymbol{q}}^{\boldsymbol{T}}$ in Eq. (2) are tensors of type $\binom{1}{0}$. To contract these two tensors to a scalar value, a quadratic form of type $\binom{0}{2}$ is needed (cf. Appendix B). The mass matrix $\boldsymbol{M(q)}$ is such a tensor, which can be seen in Eq. (10) for kinetic energy:

$$E_{kin} = \frac{1}{2}\dot{\boldsymbol{q}}^{\boldsymbol{T}}\boldsymbol{M}(\boldsymbol{q})\dot{\boldsymbol{q}}, \tag{10}$$

with $E_{kin} \in \mathbb{R}$. This means whatever joint coordinates are chosen, E_{kin} will always have the same value. Since $\boldsymbol{M(q)}$ exists for each point on the Q-manifold, it is the used metric that creates a natural bijective relation between the vector space and the co-vector space. It represents a physical quantity and is not limited to an observer-centric view (cf. Fig. 1). The set of $\dot{\boldsymbol{q}}$ satisfying

$$\dot{\boldsymbol{q}}^{\boldsymbol{T}}\boldsymbol{M}(\boldsymbol{q})\dot{\boldsymbol{q}} = 1 \tag{11}$$

is an ellipsoid in the space of joint velocities at the configuration $\boldsymbol{q}$. It is an important first result that, unlike Eq. (2), Eq. (11) indeed represents an ellipsoid in the space of joint velocities. The ellipsoid can be computed, even if not all elements of $\dot{\boldsymbol{q}}$ have the same units. However, the ellipsoid in Eq. (11) can still not be mapped in the $\mathbb{W}$-space without an inversion of $\boldsymbol{J(q)}$. From a differential geometry point of view, only if the $\mathbb{Q}$-Space and $\mathbb{W}$-Space are isomorphic, an inverse mapping exists. This is not the case for kinematically redundant robots.

For all motions, each represented by a curve passing through $\boldsymbol{q}$, a co-tangent space exists: the space of generalized joint forces $\boldsymbol{\tau} \in \mathbb{R}^n$ at $\boldsymbol{q}$. The two co-vectors $\boldsymbol{\tau}$ and $\boldsymbol{\tau}^{\boldsymbol{T}}$ are tensors of type $\binom{0}{1}$. A quadratic form of type $\binom{2}{0}$ contracts two co-vectors to a scalar value. Since $\boldsymbol{M(q)}$ is positive definite, it can always be inverted and we can use $\boldsymbol{M}(\boldsymbol{q})^{-\boldsymbol{1}}$ as a tensor of type $\binom{2}{0}$. The set of $\boldsymbol{\tau}$ satisfying

$$\boldsymbol{\tau}^{\boldsymbol{T}}\boldsymbol{M}(\boldsymbol{q})^{-\boldsymbol{1}}\boldsymbol{\tau} = 1 \tag{12}$$

is an ellipsoid in the space of generalized joint forces. We can map this ellipsoid in the $\mathbb{W}$-Space by using

$$\boldsymbol{\tau} = \boldsymbol{J}(\boldsymbol{q})^{\boldsymbol{T}}\boldsymbol{F}, \tag{13}$$

with $\boldsymbol{F} \in \mathbb{R}^m$ being the end-effector force. Substituting (13) in (12) results in the ellipsoid:

$$\boldsymbol{F}^{\boldsymbol{T}}(\boldsymbol{J}(\boldsymbol{q})\boldsymbol{M}(\boldsymbol{q})^{-\boldsymbol{1}}\boldsymbol{J}(\boldsymbol{q})^{\boldsymbol{T}})\boldsymbol{F} = 1. \tag{14}$$

Compared to the derivation of (6), no inversion of $\boldsymbol{J(q)}$ is needed. For the following parts of this work,

$$\boldsymbol{\Lambda}^{-\boldsymbol{1}} = \boldsymbol{J}(\boldsymbol{q})\boldsymbol{M}(\boldsymbol{q})^{-\boldsymbol{1}}\boldsymbol{J}(\boldsymbol{q})^{\boldsymbol{T}}, \tag{15}$$

with $\boldsymbol{\Lambda}^{-\boldsymbol{1}} \in \mathbb{R}^{m\times m}$.

3.2. Physical meaning of $\boldsymbol{\Lambda}^{-1}$

The matrix $\boldsymbol{\Lambda}^{-\boldsymbol{1}}$ incorporates a strong physical meaning. It shows the acceleration response of the manipulator to generalized forces when the manipulator is at rest:

$$\ddot{\boldsymbol{x}} = \boldsymbol{\Lambda}^{-\boldsymbol{1}}\boldsymbol{F}, \tag{16}$$

with $\ddot{\boldsymbol{x}} \in \mathbb{R}^m$ being the end-effector acceleration. Therefore, $\boldsymbol{\Lambda}^{-\boldsymbol{1}}$ is a good matrix to analyze for direct and indirect force control algorithms [31].

The matrix $\mathbf{\Lambda^{-1}}$ has already been used in robotics. In the work of Hogan, $\mathbf{\Lambda^{-1}}$ is called "mobility end-point tensor" [32]. The matrix is associated to an admittance, which has a force ("effort") as input and a motion ("flow") as output. It shows the admittance of the robot as seen from the task force. Also Khatib uses $\mathbf{\Lambda^{-1}}$ for his Operational Space Control Framework ([33,34]). In [35], $\mathbf{\Lambda^{-1}}$ was used to examine the inertial properties of the end-effector dynamics. [36] extends this work by analyzing the dynamic relation of the subtask and the main task.

None of the authors explained the differential geometric meaning of $\mathbf{\Lambda^{-1}}$: it is the induced metric in the $\mathbb{W}$-space, derived through the use of metric $\boldsymbol{M(q)}$ in the $\mathbb{Q}$-space. A direct consequence is that it is independent of the choice of joint coordinates (cf. Appendix D).

Since $\mathbf{\Lambda^{-1}}$ is a quadratic form, it is not independent of the choice of Ψ_{Task}. We will remove this dependency in the further proceeding.

3.3. Invariance on task coordinates

For $\mathbf{\Lambda^{-1}} \in \mathbb{R}^{6\times6}$, the quadratic form collects translational information, rotational information and coupling terms:

$$\mathbf{\Lambda^{-1}} = \begin{pmatrix} \mathbf{\Lambda_t^{-1}} & \mathbf{\Lambda_c^{-1}} \\ \mathbf{\Lambda_c^{-T}} & \mathbf{\Lambda_r^{-1}} \end{pmatrix}. \tag{17}$$

In the further proceeding we will neglect the coupling of rotational and translational information, represented in $\mathbf{\Lambda_c^{-1}}$.

The matrix $\mathbf{\Lambda^{-1}}$ is a tensor of type $\binom{2}{0}$. Following chapter 2.2.2, we have to transform this tensor to the type $\binom{1}{1}$ to calculate eigenvalues and eigenvectors. We can use tensor contraction to lower one index. Therefore, we need a tensor of type $\binom{0}{2}$. One choice for such a tensor $\boldsymbol{B}$ is:

$$\boldsymbol{B} = \begin{pmatrix} 0 & \beta\boldsymbol{I} \\ \beta\boldsymbol{I} & \gamma\boldsymbol{I} \end{pmatrix}, \tag{18}$$

which is an invariant quadratic form on $SE(3)$ (cf. prove in [11]). We can now apply tensor contraction:

$$\boldsymbol{\delta} = \mathbf{\Lambda^{-1}}\,\boldsymbol{B} = \begin{pmatrix} 0 & \beta\mathbf{\Lambda_t^{-1}} \\ \beta\mathbf{\Lambda_r^{-1}} & \gamma\mathbf{\Lambda_r^{-1}} \end{pmatrix} \tag{19}$$

and calculate the eigenvalues and eigenvectors of the resulting tensor $\boldsymbol{\delta} \in SE(3)$.

Even though other choices for matrix $\boldsymbol{B}$ are possible, Eq. (19) is special in that it comes with two direct advantages: firstly, we have now removed the dependency on task coordinates (cf. Appendix E); secondly, with a specific choice for $\beta \in \mathbb{R}$ and $\gamma \in \mathbb{R}$, a manipulability ellipsoid in $\mathbb{R}^3$ can be visualized. The effect of this choice can be shown by looking at the action of a wrench screw on $\boldsymbol{\delta}$. Literature on screw theory can be found in [37,38]. We can rewrite Eq. (19) to

$$\boldsymbol{\delta W} = \begin{pmatrix} 0 & \beta\mathbf{\Lambda_t^{-1}} \\ \beta\mathbf{\Lambda_r^{-1}} & \gamma\mathbf{\Lambda_r^{-1}} \end{pmatrix} \begin{pmatrix} \boldsymbol{f} \\ \boldsymbol{m} \end{pmatrix}, \tag{20}$$

with $\boldsymbol{f} \in \mathbb{R}^3$ and $\boldsymbol{m} \in \mathbb{R}^3$ being the translational and rotational part of the wrench, respectively. To this end, we can see a direct interpretation of $\boldsymbol{B}$: the scaling factors β and γ on $SE(3)$ assign a ratio between rotational and translational components of the wrench $\boldsymbol{W}$, which is represented in $\mathbb{R}^6$. To look at the action of a pure moment - a wrench screw with infinite pitch - we can set $\beta = 0$. With these explicit choice, Eq. (20) simplifies to

$$\dot{\boldsymbol{w}} = \gamma\,{\mathbf{\Lambda}_r}^{-1}\,\boldsymbol{m}, \tag{21}$$

with $\dot{\boldsymbol{w}} \in \mathbb{R}^3$ being the angular acceleration of the end-effector body. It can be seen that the pure rotation part of $\mathbf{\Lambda}^{-1}$ can be extracted for analysis:

$$\boldsymbol{\delta_r} = \gamma\,\mathbf{\Lambda_r^{-1}}, \tag{22}$$

with $\boldsymbol{\delta_r} \in \mathbb{R}^{3\times3}$. Hereby, the choice for scale factor γ on $SE(3)$ affects the chart representation of the angular acceleration in $\mathbb{R}^3$.

3.4. Manipulability ellipsoid for rotations

The manipulability for a rotational task can be visualized analyzing $\boldsymbol{\delta_r}$. Since $\boldsymbol{\delta_r}$ is a $\binom{1}{1}$-tensor, we can take eigenvalues and eigenvectors:

$$\boldsymbol{\delta_r u} = \boldsymbol{\lambda}_{\delta_r}\boldsymbol{u}_\delta. \tag{23}$$

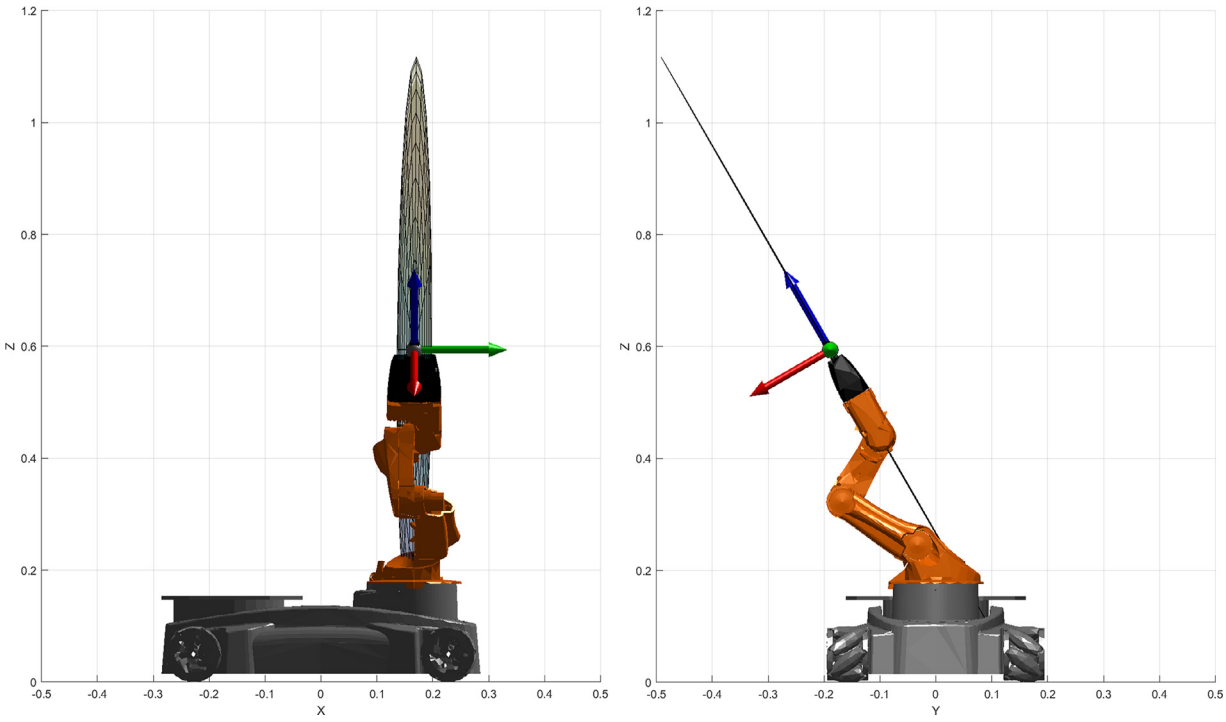

Fig. 4. *Rotational Dynamic Manipulability Ellipsoid* for a 8-DOF robot, with two translational coordinates and one rotational coordinate for the robot base and five rotational coordinates for the robot arm. The ellipsoid shows how well the robot can generate angular accelerations in respective directions of the drawn task coordinate. About the blue coordinate-axis, high angular accelerations can be produced, e.g. by turning the last joint. For angular acceleration about the green coordinate-axis, high masses have to be moved. The red coordinate-axis shows the degenerating direction (cf. yz-view right). Moving the task coordinate on the end-effector body results in the same manipulability ellipsoid (cf. Appendix E). (For interpretation of the references to colour in this figure legend, the reader is referred to the web version of this article.)

Given that $\boldsymbol{\delta_r} \in \mathbb{R}^{3\times3}$, we can plot a three-dimensional ellipsoid to describe the *Rotational Dynamic Manipulability* (cf. Fig. 4). Compared to the Velocity Manipulability Ellipsoid in Fig. 3, this ellipsoid represents a dynamic characteristic of the robot: $\boldsymbol{\delta_r}$ represents the angular acceleration after applying a moment to the end-effector body. Since $\boldsymbol{\delta_r}$ is related to the mass matrix $\boldsymbol{M(q)}$ of the robot, it shows the incorporated inertia counteracting a task moment. The angular acceleration can be visualized independent of the position of Ψ_{Task} on the end-effector body (cf. Appendix E).

4. Conclusion

Our main aim was to make the reader aware of the influence of coordinates in robotic manipulability analysis. The context is not new in differential geometry, but often disregarded in robotics. We began with an analysis of the manipulability measure $\boldsymbol{J(q)J(q)^T}$. For the design process of a robot, $\boldsymbol{J(q)J(q)^T}$ can be used to examine the robot's ability to transform joint velocities to task velocities. It therefore incorporates kinematic characteristics of the robot. We showed the limitations of this measure: $\boldsymbol{J(q)J(q)^T}$ is not comparable for users with different chart choices. Moreover, it depends on the chosen metric for the Jacobian inverse. $\boldsymbol{J(q)J(q)^T}$ cannot be used for robots with mixed joint coordinates (e.g. mobile robots).

Using tensor analysis, we removed these limitations. We showed the derivation of $\boldsymbol{\Lambda^{-1}}$, which is invariant of joint coordinates. The key features of this matrix are:

1. $\boldsymbol{\Lambda^{-1}}$ shows a physically consistent mapping between the two robotic spaces. The choice of $\boldsymbol{M(q)}$ as a metric in the $\mathbb{Q}$-space and induced metric in the $\mathbb{W}$-space enables a "natural scaling" of translational and rotational motion.
2. The matrix assigns a physical relationship to a robotic task: it shows how well a robot can resolve generalized (task) forces and therefore incorporates a dynamical characteristic.
3. The values of the matrix elements in $\boldsymbol{\Lambda^{-1}}$ are unique, no matter what set of joint coordinates are chosen to describe the kinematic structure.
4. It can also be applied to kinematically redundant robots. Hereby, the values of the matrix elements in $\boldsymbol{\Lambda^{-1}}$ are unique because no inversion of the Jacobian matrix is needed.
5. It can be used for robots with mixed joint parameters, e.g. mobile robots, without separating base and robot arm.
6. $\boldsymbol{\Lambda^{-1}}$ can be used as basis for manipulability analysis. The analysis of $\boldsymbol{\Lambda^{-1}}$ has a dependency on task coordinates.

Not all tasks can be related to a single task coordinate. We used tensor analysis to derive the coordinate invariant matrix $\boldsymbol{\delta_r}$. The key features of this matrix are:

1. $\boldsymbol{\delta_r}$ can be derived through a specific scale choice on $SE(3)$, which assigns a ratio to the rotational and translational part of the acting wrench on the end-effector body.
2. $\boldsymbol{\delta_r}$ extracts the rotational part of $\boldsymbol{\Lambda^{-1}}$. The values of the matrix elements in $\boldsymbol{\delta_r}$ are unique, no matter what joint coordinates are taken and wherever the task coordinate is placed on the end-effector body.
3. The matrix describes the dynamic ability of the robot to perform a rotational task: it shows how good the robot can transform task moments to angular accelerations.
4. The matrix can be used for manipulability analysis of purely rotational tasks. We can calculate eigenvalues and eigenvectors of $\boldsymbol{\delta_r}$ to plot a coordinate invariant *Rotational Dynamic Manipulability Ellipsoid*.

One practical limitation of the proposed manipulability measure is its use of the mass matrix $\boldsymbol{M(q)}$ as metric. For users without access to the robot dynamics extensive work has to be done to identify the data. However, multiple identification methods exist (cf. overview provided in [39]).

To analyze the manipulability of the total motion in $SE(3)$ using matrix $\boldsymbol{\delta}$ in Eq. (19), a choice for β and γ has to be made. While this work extracts the rotational component, further work can be done by decomposing the total motion into translational and rotational subgroups and analyze their respective subalgebras.

Declaration of competing interest

The authors declare that they have no known competing financial interests or personal relationships that could have appeared to influence the work reported in this paper.

Appendix A. Tensor definition

Consider a point $\boldsymbol{q}$ on a n-dimensional differentiable manifold Q. For all curves on this manifold going through point $\boldsymbol{q}$, a vector space $\mathcal{V}$ exists that collects all *contravariant elements* tangent to the curves. In the point $\boldsymbol{q}$ also a dual vector space $\mathcal{V}^*$ exists, collecting all *covariant elements*.

A.1. Covariant tensors

A covariant tensor is a multilinear function of type:

$$\boldsymbol{Q} : \underbrace{\mathcal{V} \times \ldots \times \mathcal{V}}_{s \text{ many}} \to \mathbb{R} \tag{A.1}$$

The function $\boldsymbol{Q}$ takes s many elements of $\mathcal{V}$ and returns a real number. A covariant tensor with $s = 1$ is called a co-vector.

A.2. Contravariant tensors

A contravariant tensor is a multilinear function on a covariant tensor:

$$\boldsymbol{P} : \underbrace{\mathcal{V}^* \times \ldots \times \mathcal{V}^*}_{r \text{ many}} \to \mathbb{R} \tag{A.2}$$

The function $\boldsymbol{P}$ takes r many elements of $\mathcal{V}^*$ and returns a real number. A contravariant tensor with $r = 1$ is called a vector.

A.3. Mixed tensors

Mixed tensors are r-times contravariant and s-times covariant:

$$\boldsymbol{T} : \underbrace{\mathcal{V}^* \times \ldots \times \mathcal{V}^*}_{r \text{ many}} \times \underbrace{\mathcal{V} \times \ldots \times \mathcal{V}}_{s \text{ many}} \to \mathbb{R} \tag{A.3}$$

For function $\boldsymbol{T}$ we can use the notation: $\binom{r}{s}$. The number $(r+s)$ defines the rank of the tensor. The tensor can be denoted with r many contravariant superscripts and s many covariant subscripts. For example, a $\binom{1}{1}$-tensor with rank 2 has one contravariant superscript i and one covariant superscript j: $\boldsymbol{T}^i_j$.

Appendix B. Example of tensor contraction

Operations on tensors can be illustrated with an example:

$$\boldsymbol{\eta_k} = \boldsymbol{g_{ik}}\boldsymbol{\xi^i}, \tag{B.1}$$

with $i = k = 1, \ldots, n$. On the right side of Eq. (B.1), a contravariant tensor $\boldsymbol{\xi^i}$ and a twice covariant tensor $\boldsymbol{g_{ik}}$ appears. The left side yields a covariant tensor $\boldsymbol{\eta_k}$. The operation on the appearing tensors can be seen: the tensor $\boldsymbol{g_{ik}}$ is used to transform the contravariant tensor $\boldsymbol{\xi^i}$ to a covariant tensor $\boldsymbol{\eta_k}$. This operation on tensors is called *contraction*. Contraction sums pairs of equal indices, which are one upper (contravariant) index and one lower (covariant) index:

$$\boldsymbol{\eta_k} = \sum_{i=1}^{n} \boldsymbol{g_{ik}}\boldsymbol{\xi^i}. \tag{B.2}$$

As a result, the index can be canceled out. Implicitly, the sum symbol is left out.

Appendix C. $\boldsymbol{J(q)J(q)^T}$ for different sets of joint coordinates

Figs. 2 and 3 show a 3-DOF planar robot, with parameters

- $l_1 = l_2 = l_3 = 1\ m$ (Link lengths)
- $p_{l_1} = p_{l_2} = p_{l_3} = 0.5\ m$ (Center of gravity)
- $m_1 = m_2 = m_3 = 1\ kg$ (Link masses)
- $I_1 = I_2 = I_3 = 1\ kgm^2$ (Inertia of links),

different joint coordinates

- Joint coordinate set 1: $\theta_1 = \frac{\pi}{9}\ rad,\ \theta_2 = \frac{\pi}{4}\ rad,\ \theta_3 = \frac{\pi}{3}\ rad$
- Joint coordinate set 2: $p_1 = 0.34\ m,\ p_2 = 0.71\ m,\ p_3 = 0.87\ m$
- Joint coordinate set 3: $\theta_1 = \frac{\pi}{9}\ rad,\ \theta_2 = \frac{\pi}{4}\ rad,\ p_3 = 0.87\ m$

and randomly chosen weightening matrix $\boldsymbol{W_{rand}} = \begin{pmatrix} 3.00 & 0.00 & 0.00 \\ 0.00 & 0.3 & 0.00 \\ 0.00 & 0.00 & 0.03 \end{pmatrix}$. The Jacobian matrices for joint coordinate set $1-3$ in the given configuration are

- $\boldsymbol{J(q)}_1 = \begin{pmatrix} -2.07\ \frac{m}{rad} & -1.73\ \frac{m}{rad} & -0.82\ \frac{m}{rad} \\ 0.79\ \frac{m}{rad} & -0.15\ \frac{m}{rad} & -0.57\ \frac{m}{rad} \end{pmatrix}$
- $\boldsymbol{J(q)}_2 = \begin{pmatrix} -2.20 & -2.44 & -1.64 \\ 0.84 & -0.21 & -1.15 \end{pmatrix}$
- $\boldsymbol{J(q)}_3 = \begin{pmatrix} -2.07\ \frac{m}{rad} & -1.73\ \frac{m}{rad} & -1.64 \\ -0.79\ \frac{m}{rad} & -0.15\ \frac{m}{rad} & -1.15 \end{pmatrix}$

respectively. Consequently, $\boldsymbol{J(q)J(q)^T}$ for each joint coordinate set yields

- $\boldsymbol{J(q)J(q)^T}_1 = \begin{pmatrix} 7.92\ \frac{m^2}{rad^2} & -0.90\ \frac{m^2}{rad^2} \\ -0.90\ \frac{m^2}{rad^2} & 0.97\ \frac{m^2}{rad^2} \end{pmatrix}$
- $\boldsymbol{J(q)J(q)^T}_2 = \begin{pmatrix} 13.48 & 0.55 \\ 0.55 & 2.07 \end{pmatrix}$
- $\boldsymbol{J(q)J(q)^T}_3 = \begin{pmatrix} 7.28\frac{m^2}{rad^2} + 2.69 & -1.38\frac{m^2}{rad^2} + 1.89 \\ -1.38\frac{m^2}{rad^2} + 1.89 & 0.65\frac{m^2}{rad^2} + 1.32 \end{pmatrix}$.

The respective eigenvalues and eigenvectors of $\boldsymbol{J(q)J(q)^T}_1$ and $\boldsymbol{J(q)J(q)^T}_2$ are different:

- Eigenvalues of $\boldsymbol{J(q)J(q)^T}_1$: $\lambda_1 = 0.86, \lambda_2 = 8.04$
- (Right) Eigenvectors of $\boldsymbol{J(q)J(q)^T}_1$: $u_1 = \begin{pmatrix} -0.13 \\ -0.99 \end{pmatrix}, u_2 = \begin{pmatrix} -0.99 \\ 0.13 \end{pmatrix}$
- Eigenvalues of $\boldsymbol{J(q)J(q)^T}_2$: $\lambda_1 = 13.51, \lambda_2 = 2.04$
- (Right) Eigenvectors of $\boldsymbol{J(q)J(q)^T}_2$: $u_1 = \begin{pmatrix} 0.05 \\ -1.00 \end{pmatrix}, u_2 = \begin{pmatrix} -1.00 \\ -0.05 \end{pmatrix}$

Matrix $\boldsymbol{J(q)J(q)^T}_3$ can not be calculated, because a mismatch of units arises.

Appendix D. Induced metric $\boldsymbol{\Lambda^{-1}}$

The mass matrices for joint coordinate set $1-3$ in the given configuration are

- $\boldsymbol{M(q)}_1 = \begin{pmatrix} 9.11\ \frac{kgm^2}{rad} & 4.93\ \frac{kgm^2}{rad} & 1.37\ \frac{kgm^2}{rad} \\ 4.93\ \frac{kgm^2}{rad} & 4.00\ \frac{kgm^2}{rad} & 1.50\ \frac{kgm^2}{rad} \\ 1.37\ \frac{kgm^2}{rad} & 1.50\ \frac{kgm^2}{rad} & 1.25\ \frac{kgm^2}{rad} \end{pmatrix}$
- $\boldsymbol{M(q)}_2 = \begin{pmatrix} 10.32\ kg & 7.42\ kg & 2.92\ kg \\ 7.42\ kg & 8.00\ kg & 4.24\ kg \\ 2.92\ kg & 4.24\ kg & 5.00\ kg \end{pmatrix}$
- $\boldsymbol{M(q)}_3 = \begin{pmatrix} 9.11\ \frac{kgm^2}{rad} & 4.93\ \frac{kgm^2}{rad} & 2.74\ kgm \\ 4.93\ \frac{kgm^2}{rad} & 4.00\ \frac{kgm^2}{rad} & 3.00\ kgm \\ 2.74\ kgm & 3.00\ kgm & 5.00\ kg \end{pmatrix}$

respectively. Consequently, the matrix $\boldsymbol{\Lambda}^{-1}$ for each set of joint coordinates yields $\boldsymbol{\Lambda}_1^{-1} = \boldsymbol{\Lambda}_2^{-1} = \boldsymbol{\Lambda}_3^{-1} = \boldsymbol{J(q)}_1\boldsymbol{M(q)}_1^{-1}\boldsymbol{J(q)}_1^T = \boldsymbol{J(q)}_2\boldsymbol{M(q)}_2^{-1}\boldsymbol{J(q)}_2^T = \boldsymbol{J(q)}_3\boldsymbol{M(q)}_3^{-1}\boldsymbol{J(q)}_3^T = \begin{pmatrix} 0.79\ \frac{1}{kg} & 0.18\ \frac{1}{kg} \\ 0.18\ \frac{1}{kg} & 0.53\ \frac{1}{kg} \end{pmatrix}$. It can be seen that the matrix products are equal.

Appendix E. Invariant matrix $\boldsymbol{\delta_r}$

Fig. 4 shows a 8-DOF robot with joint coordinate set:

$p_1 = 0\ m,\ p_2 = 0\ m,\ \theta_1 = 0\ rad,\ \theta_2 = -\frac{pi}{2}\ rad,\ \theta_3 = \frac{pi}{3}\ rad,\ \theta_4 = -\frac{pi}{2}\ rad,\ \theta_5 = \frac{pi}{3}\ rad,\ \theta_6 = 0\ rad$, and two different task coordinates Ψ_1 and Ψ_2 on end-effector body. The respective homogeneous transformation matrices $\boldsymbol{H}_1^0 \in SE(3)$ of Ψ_1 and $\boldsymbol{H}_2^0 \in SE(3)$ of Ψ_2 are:

- $\boldsymbol{H}_1^0 = \begin{pmatrix} 0.00 & 1 & 0 & 0.17\ m \\ -0.87 & 0 & -0.50 & -0.19\ m \\ -0.50 & 0 & 0.87 & 0.59\ m \\ 0 & 0 & 0 & 1 \end{pmatrix}$
- $\boldsymbol{H}_2^0 = \begin{pmatrix} 0.50 & 0.87 & 0 & 0.20\ m \\ -0.75 & 0.43 & -0.50 & -0.21\ m \\ -0.44 & 0.25 & 0.87 & 0.56\ m \\ 0 & 0 & 0 & 1 \end{pmatrix}$

The Jacobian matrices for the two task coordinates Ψ_1 and Ψ_2 for the given joint coordinate set are

$$\cdot\, \boldsymbol{J(q)}_1 = \begin{pmatrix} 1 & 0 & 0.19\ \frac{m}{rad} & 0.19\ \frac{m}{rad} & 0\ \frac{m}{rad} & 0\ \frac{m}{rad} & 0\ \frac{m}{rad} & 0\ \frac{m}{rad} \\ 0 & 1 & 0.17\ \frac{m}{rad} & 0\ \frac{m}{rad} & -0.35\ \frac{m}{rad} & -0.27\ \frac{m}{rad} & -0.15\ \frac{m}{rad} & 0\ \frac{m}{rad} \\ 0 & 0 & 0\ \frac{m}{rad} & 0\ \frac{m}{rad} & -0.16\ \frac{m}{rad} & -0.02\ \frac{m}{rad} & -0.09\ \frac{m}{rad} & 0\ \frac{m}{rad} \\ 0\ \frac{rad}{m} & 0\ \frac{rad}{m} & 0 & 0 & 1 & 1 & 1 & 0 \\ 0\ \frac{rad}{m} & 0\ \frac{rad}{m} & 0 & 0 & 0 & 0 & 0 & -0.50 \\ 0\ \frac{rad}{m} & 0\ \frac{rad}{m} & 1 & 1 & 0 & 0 & 0 & 0.87 \end{pmatrix}$$

$$\cdot\, \boldsymbol{J(q)}_2 = \begin{pmatrix} 1 & 0 & 0.21\ \frac{m}{rad} & 0.21\ \frac{m}{rad} & 0\ \frac{m}{rad} & 0\ \frac{m}{rad} & 0\ \frac{m}{rad} & 0.04\ \frac{m}{rad} \\ 0 & 1.00 & 0.20\ \frac{m}{rad} & 0.04\ \frac{m}{rad} & -0.32\ \frac{m}{rad} & -0.24\ \frac{m}{rad} & -0.12\ \frac{m}{rad} & 0.03\ \frac{m}{rad} \\ 0 & 0 & 0\ \frac{m}{rad} & 0\ \frac{m}{rad} & -0.18\ \frac{m}{rad} & -0.04\ \frac{m}{rad} & -0.11\ \frac{m}{rad} & 0.02\ \frac{m}{rad} \\ 0\ \frac{rad}{m} & 0\ \frac{rad}{m} & 0 & 0 & 1 & 1 & 1 & 0 \\ 0\ \frac{rad}{m} & 0\ \frac{rad}{m} & 0 & 0 & 0 & 0 & 0 & -0.50 \\ 0\ \frac{rad}{m} & 0\ \frac{rad}{m} & 1 & 1 & 0 & 0 & 0 & 0.87 \end{pmatrix}$$

The mass matrix in the given configuration is

$$\boldsymbol{M}(\boldsymbol{q}) = \begin{pmatrix} 31.57\ kg & 0\ kg & 0.54\ kgm & 0.54\ kgm \\ 0\ kg & 31.57\ kg & 1.06\ kgm & 0.03\ kgm \\ 0.54\ kgm & 1.06\ kgm & 1.27\ \frac{kgm^2}{rad} & 0.09\ \frac{kgm^2}{rad} \\ 0.54\ kgm & 0.03\ kgm & 0.09\ \frac{kgm^2}{rad} & 0.08\ \frac{kgm^2}{rad} \\ 0\ kgm & -0.70\ kgm & -0.12\ \frac{kgm^2}{rad} & 6.44\text{e-}5\ \frac{kgm^2}{rad} \\ 0\ kgm & -0.41\ kgm & -0.07\ \frac{kgm^2}{rad} & 0.14\text{e-}2\ \frac{kgm^2}{rad} \\ 0\ kgm & -0.14\ kgm & -0.02\ \frac{kgm^2}{rad} & 7.82\text{e-}4\ \frac{kgm^2}{rad} \\ 0\ kgm & 7.14\text{e-}4\ kgm & 3.59\text{e-}4\ \frac{kgm^2}{rad} & 2.39\text{e-}4\ \frac{kgm^2}{rad} \end{pmatrix}$$

$$\begin{pmatrix} 0\ kgm & 0\ kgm & 0\ kgm & 0\ kgm \\ -0.70\ kgm & -0.41\ kgm & -0.14\ kgm & 7.14\text{e-}4\ kgm \\ -0.12\ \frac{kgm^2}{rad} & -0.07\ \frac{kgm^2}{rad} & -0.02\ \frac{kgm^2}{rad} & 3.59\text{e-}4\ \frac{kgm^2}{rad} \\ 6.44\text{e-}5\ \frac{kgm^2}{rad} & 0.14\text{e-}2\ \frac{kgm^2}{rad} & 7.82\text{e-}4\ \frac{kgm^2}{rad} & 2.39\text{e-}4\ \frac{kgm^2}{rad} \\ 0.20\ \frac{kgm^2}{rad} & 0.10\ \frac{kgm^2}{rad} & 0.05\ \frac{kgm^2}{rad} & -2.76\text{e-}4\ \frac{kgm^2}{rad} \\ 0.10\ \frac{kgm^2}{rad} & 0.08\ \frac{kgm^2}{rad} & 0.03\ \frac{kgm^2}{rad} & -1.65\text{e-}4\ \frac{kgm^2}{rad} \\ 0.05\ \frac{kgm^2}{rad} & 0.03\ \frac{kgm^2}{rad} & 0.02\ \frac{kgm^2}{rad} & -1.09\text{e-}4\ \frac{kgm^2}{rad} \\ -2.76\text{e-}4\ \frac{kgm^2}{rad} & -1.65\text{e-}4\ \frac{kgm^2}{rad} & -1.09\text{e-}4\ \frac{kgm^2}{rad} & 2.76\text{e-}4\ \frac{kgm^2}{rad} \end{pmatrix}$$

The matrix $\boldsymbol{\delta_r}$ for task coordinate Ψ_1 and Ψ_2 yields

$$\boldsymbol{\delta_r} = \boldsymbol{\delta_{r1}} = \boldsymbol{\delta_{r2}} = \begin{pmatrix} 92.80\ \frac{rad}{kgm^2} & -11.27\ \frac{rad}{kgm^2} & 18.21\ \frac{rad}{kgm^2} \\ -11.27\ \frac{rad}{kgm^2} & 909.38\ \frac{rad}{kgm^2} & -1568.90\ \frac{rad}{kgm^2} \\ 18.21\ \frac{rad}{kgm^2} & -1568.90\ \frac{rad}{kgm^2} & 2720.70\ \frac{rad}{kgm^2} \end{pmatrix}$$

Consequently, the respective Eigenvalues and Eigenvectors of $\boldsymbol{\delta_r}$ are the same:

- Eigenvalues: $\lambda_1 = 0.37,\ \lambda_2 = 9.54\text{e-}4,\ \lambda_3 = 1.34\text{e-}6$
- (Right) Eigenvectors: $u_1 = \begin{pmatrix} -0.01 \\ 0.50 \\ -0.87 \end{pmatrix}, u_2 = \begin{pmatrix} -1.00 \\ 0.00 \\ 0.01 \end{pmatrix}, u_3 = \begin{pmatrix} 0.01 \\ 0.86 \\ 0.50 \end{pmatrix}$

References

[1] C. Chevallereau, B. Daya, A new method for robot control in singular configurations with motion in any cartesian direction, in: Proceedings of the 1994 IEEE International Conference on Robotics and Automation, 4, 1994, pp. 2692–2697, doi:10.1109/ROBOT.1994.350929.

[2] N. Vahrenkamp, T. Asfour, G. Metta, G. Sandini, R. Dillmann, Manipulability analysis, in: 12th IEEE-RAS International Conference on Humanoid Robots, 12, 2012, pp. 568–573, doi:10.1109/HUMANOIDS.2012.6651576.

[3] O. Egeland, M. Ebdrup, S. Chiaverini, Sensory control in singular configurations application to visual servoing, in: Proceedings of the IEEE International Workshop on Intelligent Motion Control, 2, 1990, pp. 401–406, doi:10.1109/IMC.1990.687352.

[4] H. Sadeghian, F. Zokaei, S. Hadian Jazi, Constrained kinematic control in minimally invasive robotic surgery subject to remote center of motion constraint, J. Intell. Robot. Syst. 95 (3–4) (2019) 901–913, doi:10.1007/s10846-018-0927-0.

[5] H. Asada, A geometrical representation of manipulator dynamics and its application to arm design, J. Dyn. Syst. Meas.Control 105 (3) (1983) 131, doi:10.1115/1.3140644.

[6] B.W. Choi, J.H. Won, M.J. Chung, Evaluation of dexterity measures for a 3-link planar redundant manipulator using constraint locus, IEEE Trans. Robot. Autom. 11 (2) (1995) 282–285, doi:10.1109/70.370510.

[7] P.H. Chang, A dexterity measure for kinematic control of redundant manipulators, in: Proceedings of the 1989 American Control Conference, 2, 1989, pp. 496–502, doi:10.23919/ACC.1989.4790242.

[8] J. Eden, D. Lau, Y. Tan, D. Oetomo, Unilateral manipulability quality indices: generalized manipulability measures for unilaterally actuated robots, J. Mech. Des. 141 (9) (2019) 161, doi:10.1115/1.4043932.

[9] O. Ma, J. Angeles, Optimum architecture design of platform manipulators, in: International Conference on Advanced Robotics 'Robots in Unstructured Environments, 5, 1991, pp. 1130–1135 vol.2, doi:10.1109/ICAR.1991.240404.

[10] J. Angeles, Fundamentals of robotic mechanical systems: Theory, methods, and algorithms, Mechanical engineering series, 4. ed., Springer, Cham, 2014.

[11] , A Mathematical Introduction to Robotic Manipulation, R.M. Murray, Z. Li, S.S. Sastry (Eds.), CRC Press, Boca Raton, 1994.

[12] J.K. Salisbury, J.J. Craig, Articulated hands: force control and kinematic issues, Int. J. Robot. Res. 1 (1) (1982) 4–17, doi:10.1177/027836498200100102.

[13] R.P. Paul, C.N. Stevenson, Kinematics of robot wrists, Int. J. Robot. Res. 2 (1) (1983) 31–38, doi:10.1177/027836498300200103.

[14] C.A. Klein, B.E. Blaho, Dexterity measures for the design and control of kinematically redundant manipulators, Int. J. Robot. Res. 6 (2) (1987) 72–83, doi:10.1177/027836498700600206.

[15] J. Baillieul, A constraint oriented approach to inverse problems for kinematically redundant manipulators, in: Proceedings of the 1987 IEEE International Conference on Robotics and Automation, 1, 1987, pp. 1827–1833, doi:10.1109/ROBOT.1987.1087809.

[16] J.-O. Kim, K. Khosla, Dexterity measures for design and control of manipulators, in: Proceedings IROS '91:IEEE/RSJ International Workshop on Intelligent Robots and Systems, 1, 1991, pp. 758–763, doi:10.1109/IROS.1991.174572.

[17] S.L. Chiu, Task compatibility of manipulator postures, Int. J. Robot. Res. 1 (5) (1988) 13–21, doi:10.1177/027836498800700502.

[18] F. Burget, M. Bennewitz, Stance selection for humanoid grasping tasks by inverse reachability maps, in: Proceedings of the 2015 IEEE International Conference on Robotics and Automation, 1, 2015, pp. 5669–5674, doi:10.1109/ICRA.2015.7139993.

[19] F. Chen, M. Selvaggio, D.G. Caldwell, Dexterous grasping by manipulability selection for mobile manipulator with visual guidance, IEEE Trans. Ind. Inform. 15 (2) (2019) 1202–1210, doi:10.1109/TII.2018.2879426.
[20] J. Duan, Y. Gan, P. Cao, X. Dai, The optimal solution for base frame installation of dual-arm robot, Int. Conf. Adv. Robot.Mechatron. (ICARM) 4 (2019) 546–552, doi:10.1109/ICARM.2019.8833952.
[21] H. Su, S. Li, J. Manivannan, L. Bascetta, G. Ferrigno, E.D. Momi, Manipulability optimization control of a serial redundant robot for robot-assisted minimally invasive surgery, Int. Conf. Robot.Autom. 1 (2019) 1323–1328, doi:10.1109/ICRA.2019.8793676.
[22] T. Yoshikawa, Manipulability of robotic mechanisms, Int. J. Robot. Res. 4 (2) (1985) 3–9, doi:10.1177/027836498500400201.
[23] T. Yoshikawa, Dynamic manipulability of robot manipulators, in: Proceedings of the 1985 International Conference on Robotics and Automation, 1, 1985, pp. 1033–1038, doi:10.1109/ROBOT.1985.1087277.
[24] C.A. Klein, C.-H. Huang, Review of pseudoinverse control for use with kinematically redundant manipulators, IEEE Trans. Syst. Man Cybern. SMC-13 (2) (1983) 245–250, doi:10.1109/TSMC.1983.6313123.
[25] E.M. Schwartz, R. Manseur, K.L. Doty, Noncommensurate systems in robotics, Int. J. Robot. Autom. (2002).
[26] J.-P. Merlet, Jacobian, manipulability, condition number and accuracy of parallel robots, J. Mech. Des. 1 (128) (2006) 199–206, doi:10.1007/978-3-540-48113-3_16.
[27] M. Azad, J. Babič, M. Mistry, Effects of the weighting matrix on dynamic manipulability of robots, Autonom. Robots 43 (7) (2019) 1867–1879, doi:10.1007/s10514-018-09819-y.
[28] B.A. Dubrovin, A.T. Fomenko, S.P. Novikov, Modern Geometry - Methods and Applications, 93, Springer New York, New York, 1984, doi:10.1007/978-1-4684-9946-9.
[29] W.M. Boothby, An introduction to differentiable manifolds and Riemannian geometry, Pure and applied mathematics, 63, Academic Press, New York, 1975.
[30] T. Frankel, The Geometry of Physics, Cambridge University Press, Cambridge, 2011, doi:10.1017/CBO9781139061377.
[31] L.S. Wilfinger, A comparison of force control algorithms for robots in contact with flexible environments, Cirsse Report, 135, NASA, New York, 1992.
[32] N. Hogan, Impedance control of industrial robots, Robot. Comput.-Integr. Manuf. 1 (1) (1984) 97–113, doi:10.1016/0736-5845(84)90084-X.
[33] O. Khatib, Commande dynamique dans l'espace operationnel des robots manipulateurs en presence d'obstacles, Universite Paul Sabatier, Toulouse, 1980 Ph.D. thesis.
[34] O. Khatib, A unified approach for motion and force control of robot manipulators: the operational space formulation, IEEE J. Robot. Autom. 3 (1) (1987) 43–53, doi:10.1109/JRA.1987.1087068.
[35] O. Khatib, Inertial properties in robotic manipulation: an object-level framework, Int. J. Robot. Res. 14 (1) (1995) 19–36, doi:10.1177/027836499501400103.
[36] O. Khatib, L. Sentis, Whole-body dynamic behavior and control of human-like robots, Int. J. Humanoid Robot. 01 (01) (2004) 29–43, doi:10.1142/S0219843604000058.
[37] R.S. Ball, A Treatise on the Theory of Screws, Cambridge University Press (1900).
[38] S. Stramigioli, B. Maschke, C. Bidard, On the geometry of rigid-body motions: the relation between lie groups and screws, Proc. Inst. Mech.Eng. Part C: J. Mech. Eng. Sci. 216 (1) (2002) 13–23, doi:10.1243/0954406021524873.
[39] B. Siciliano, O. Khatib, Springer Handbook of Robotics, B. Siciliano, O. Khatib (Eds.), Springer Science and Business Media, Berlin, 2008.